A tool for reducing cone-beam artifacts in computed tomography data

Evelina Ametova, Massimiliano Ferrucci, Wim Dewulf

KU Leuven, Mechanical Engineering Department, Celestijnenlaan 300, 3001 Leuven, Belgium

email: evelina.ametova@kuleuven.be, massimiliano.ferrucci@kuleuven.be, wim.dewulf@kuleuven.be

Abstract

Cone-beam computed tomography (CT) with circular scanning trajectory is known to suffer from so called cone-beam artifacts. Cone-beam artifacts are errors in the reconstructed volume due to incomplete radon data. These artifacts increase with increasing distance of the reconstructed plane from the midplane, *i.e.* the plane containing the X-ray source. Theoretically, the midplane represents the ideal data set for tomographic reconstruction as the entire set of line integrals, *i.e.* the X-ray attenuation trajectories, are parallel to the plane they are used to reconstruct. The angle between the reconstructed plane and the line integrals used to reconstruct it increases with increasing distance from the midplane. Cone-beam artifacts generally result in a degradation of tomographically reconstructed edges, subsequently affecting dimensional measurements. Appearance of cone-beam artifacts depends on the position and orientation of the object under investigation in the measurement volume.

In this paper we propose an algorithm that takes as an input the triangulated surface, *e.g.* a CAD model, of a scanned object and predicts where the object's surface cannot be reconstructed properly due to cone-beam artifacts. We apply Tuy's data sufficiency condition to define the analytical relationship between each surface triangle in the object model and the ability to reconstruct it using circular scan CT. The output of the proposed algorithm is the object position and orientation that reduces the effects of cone beam artifacts. The proposed algorithm is highly parallelizable and provides computational benefits when compared to conventional CT simulation methods. Operators of CT can use the proposed algorithm to reduce the influence of cone-beam artifacts on measurement results.

Keywords: Cone-beam Artifacts, Triangulated Surface, Data Sufficiency Condition

1 Introduction

Acquisition of CT data with a cone-shaped X-ray beam and a 2D detector is generally faster when compared to, for example, a fan-shaped beam and a 1D detector. For industrial CT systems, the object is placed between the X-ray source and the detector on the computer-controlled rotation stage and 2D radiographs are acquired for various rotation positions, typically covering a full 360º revolution, of the object. The set of 2D radiographs and the corresponding object orientation are used to tomographically reconstruct the object as a 3D attenuation map. A common algorithm used for tomographic reconstruction from 2D radiographs is the Feldkamp-Davis-Kress (FDK) method. Image segmentation based on the difference in the attenuation values is used to extract surfaces, *i.e*. object boundaries, and perform dimensional quality control of the object under investigation. From a dimensional metrology point of view, an object's dimensions can be fully defined by its surface. Consequently, the accurate reconstruction of an object's surface is critical for performing accurate dimensional measurements.

Cone-beam artifacts are inherent to the scanning geometry of cone-beam CT with circular trajectory due to violation of the data sufficiency condition formulated by Tuy in [1]. According to Tuy's condition, accurate reconstruction of a plane requires that the plane contains the X-ray focal spot point. Tuy's condition can be illustrated as follows. Let $\boldsymbol{x}$ be a point in the cone-beam CT measurement volume and $\boldsymbol{s}$ be the X-ray focal spot at a given rotation position α of the object. Depending on the position of the point in the volume, there will be a set of planes which cannot be measured with the circular scanning geometry (figure 1a). Non-measurable planes are defined by the set of normals contained within **H**.

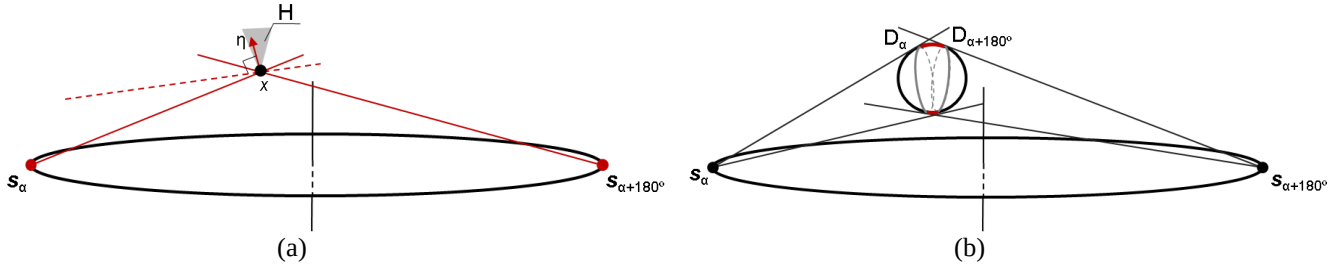

(a) (b)

Figure 1. (a) Schematic illustration of geometrical restrictions in reconstructing certain surfaces using circular cone-beam CT resulting in cone-beam artifacts. For better visualization, the illustration is restricted to one plane. The non-measurable plane is shown as a dashed red line. A set of non-measurable plane normals for point $\boldsymbol{x}$ *is shown in shaded region* **H**. *Figure is adapted from reference [2]. (b) Illustration of the influence of cone-beam artifacts on the 3D imaging of a sphere. Sphere silhouettes are shown in grey. Surfaces that cannot be accurately reconstructed are shown in red at the top and bottom of the sphere.*

2 Method

2.1 Model

Let us start by considering a single-material object $f(\boldsymbol{b})$, which is a collection of all points $\boldsymbol{b} = (b_x, b_y, b_z)$ contained within a surface $\mathcal{S}$, such that $f(\boldsymbol{b}) = 1$ if point $\boldsymbol{b}$ is inside $\mathcal{S}$and $f(\boldsymbol{b}) = 0$ otherwise. For a given rotation position α, the ideal projection of the object will provide us with a contour $\mathcal{C}$ that encloses all non-background points on the projection, *i.e.* the projection support. The contour $\mathcal{C}$ is built by the set of cone-beam X-rays that are tangent to object's surface. Consequently, knowledge of this contour is equivalent to knowledge of the object's silhouette $\mathcal{D}$ at this rotation position, *i.e.* the cross-sectional edge traced by a tangent cone, the vertex of which is the X-ray focal spot (figure 1b). Tomographic reconstruction of the surface $\mathcal{S}$ can be understood as the collection of silhouettes $\mathcal{D}_\alpha$ from all rotation angles $\alpha \in [0{,}360°]$. Accurate surface reconstruction requires that, for every surface point $\boldsymbol{p} \in \mathcal{S}$, there is a corresponding contour point $\boldsymbol{u} \in \mathcal{C}$; otherwise, the surface in $\boldsymbol{p} \notin \mathcal{D}_\alpha, \forall\alpha$ and the surface in $\boldsymbol{p}$ cannot be accurately reconstructed. Point $\boldsymbol{p}$ will have a corresponding contour point $\boldsymbol{u}$ if the surface normal $\boldsymbol{n_p} \notin \mathbf{H}$, *i.e.* if there is any rotation position α for which the X-ray originating from source $\boldsymbol{s}$ is tangent to the surface at $\boldsymbol{p}$. Let us denote the position of the X-ray focal spot as $\boldsymbol{s} = (s_x, s_y, s_z)$, source-to-rotation axis distance as L, and the surface point as $\boldsymbol{p} = (p_x, p_y, p_z)$ with corresponding surface normal $\boldsymbol{n} = (n_x, n_y, n_z,)$. A rotation of α about the rotation axis Y is given by the following matrix:

$$\boldsymbol{R_\alpha} = \begin{bmatrix} \cos\alpha & 0 & -\sin\alpha \\ 0 & 1 & 0 \\ \sin\alpha & 0 & \cos\alpha \end{bmatrix}. \tag{1}$$

The rotation matrix in equation *(1)* is left multiplied into $\boldsymbol{p}$ to produce a new rotated coordinate position $\boldsymbol{p_\alpha}$ as follows.

$$\boldsymbol{p_\alpha} = \boldsymbol{R_\alpha p}. \tag{2}$$

The normal vector $\boldsymbol{n_\alpha}$ at point $\boldsymbol{p_\alpha}$ in the rotated surface point is then given by equation *(3)*.

$$\boldsymbol{n_\alpha} = \boldsymbol{R_\alpha n}. \tag{3}$$

The tangent planes passing through point $\boldsymbol{p_\alpha}$ and focal point $\boldsymbol{s} = (s_x, s_y, s_z)$ can be parameterized as follows.

$$n_x\,(p_x - s_x) + n_y\,(p_y - s_y) + n_z\,(p_z - s_z) = 0. \tag{4}$$

Substituting equations *(2)* and *(3)* into equation *(4)*, we deduce the parameterized tangent plane for $\boldsymbol{p_\alpha}$ as follows:

$$\begin{gathered}(n_x\cos\alpha + n_z\sin\alpha)(p_x\cos\alpha + p_z\sin\alpha - s_x) + n_y(p_y - s_y) + \\ +(-n_x\sin\alpha + n_z\cos\alpha)(-p_x\sin\alpha + p_z\cos\alpha + L - s_z) = 0.\end{gathered} \tag{5}$$

Rearranging the terms of equation *(5)* provides the following expression.

$$\begin{gathered}p_x\,n_x\,(\sin^2\alpha + \cos^2\alpha) + p_z\,n_z\,(\sin^2\alpha + \cos^2\alpha) - s_x\,n_x\cos\alpha - s_x\,n_z\sin\alpha + n_y\,(p_y - s_y) + \\ +s_z\,n_x\sin\alpha - s_z\,n_z\cos\alpha - L\,n_x\sin\alpha + L\,n_z\cos\alpha = 0.\end{gathered} \tag{6}$$

Using trigonometric relation $(\sin^2\alpha + \cos^2\alpha) = 1$, equation *(6)* reduces to equation *(7)*.

$$p_x\,n_x + p_z\,n_z\, - s_x\,n_x\cos\alpha - s_x\,n_z\sin\alpha + n_y\,(p_y - s_y) + s_z\,n_x\sin\alpha - s_z\,n_z\cos\alpha - L\,n_x\sin\alpha + L\,n_z\cos\alpha = 0. \tag{7}$$

We can rewrite equation *(7)* as:

$$a\sin\alpha + b\cos\alpha = c, \tag{8}$$

where

$$\begin{aligned} a &= s_x\,n_z - s_z\,n_x + L\,n_x, \\ b &= s_x\,n_x + s_z\,n_z - L\,n_z, \\ c &= p_x\,n_x + n_y\,(p_y - s_y) + p_z\,n_z\,. \end{aligned} \tag{9}$$

Solving equation (8) for α gives us:

$$\alpha = \pm \cos^{-1} \frac{c}{\sqrt{a^2 + b^2}} + \tan^{-1} \frac{b}{a} \quad (10)$$

The $\cos^{-1}$ term is restricted to the domain $[-1,1]$. Consequently, equation *(10)* has a solution only if:

$$-1 \leq \frac{c}{\sqrt{a^2 + b^2}} \leq 1, \quad (11)$$

which simplifies to:

$$a^2 + b^2 \geq c^2. \quad (12)$$

Hence, point $\boldsymbol{p}$ with normal $\boldsymbol{n}$ will have the corresponding contour point $\boldsymbol{u}$ at rotation position α only if equation *(13)* is satisfied:

$$(s_x\, n_z - s_z\, n_x + L\, n_x)^2 + (s_x\, n_z - s_z\, n_x + L\, n_x)^2 \geq \left(p_x\, n_x + n_y \left(p_y - s_y\right) + p_z\, n_z\right)^2 \quad (13)$$

2.2 Implementation

We developed a simulation tool that takes as input an STL file and, based on the method described in previous section, determines which triangles in the STL mesh satisfy equation *(13)* for a given rotation position α. The triangles that do not satisfy condition *(13)* are identified and the surface area that cannot be properly reconstructed is calculated. We use color mapping to show which triangles cannot be reconstructed. In the general case, there exist multiple object orientations where cone-beam artifacts will have insignificant influence. The simulation tool allows the CT system operator to specify an initial object orientation by way of exact Euler angles or a range of these angles. From these initial values, the simulation tool finds the set of object orientations that minimize the surface area that cannot be properly reconstructed.

3 Results

In this section we demonstrate some capabilities of developed simulation tool with a case study.To evaluate proposed method, we simulated several CT scans of the part shown in figure 2 in different orientations. High resolution mesh of 4300748 was used for simulations and subsequent calculations. We selected 12 orientations of the test object (figure 3). For simplicity, the object was rotated about one axis (horizontal axis parallel to the detector) with 10° steps; the other two other rotation angles were fixed.

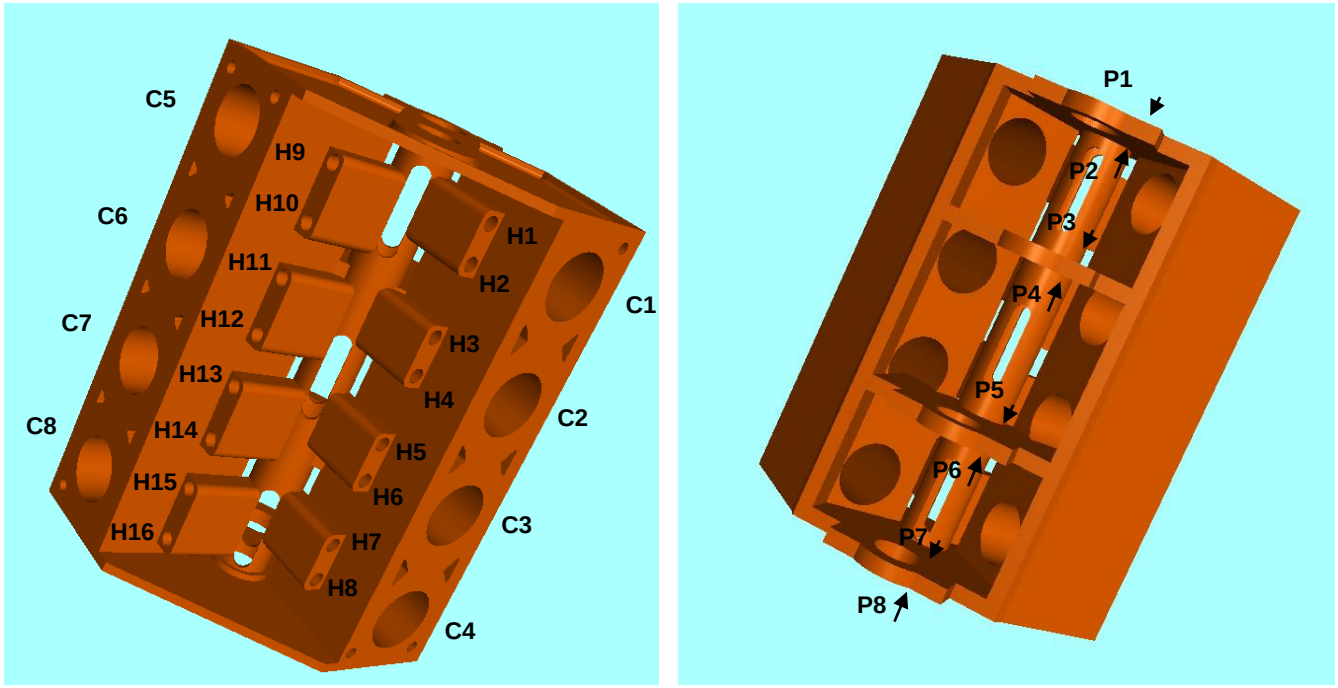

Figure 2. Test object.

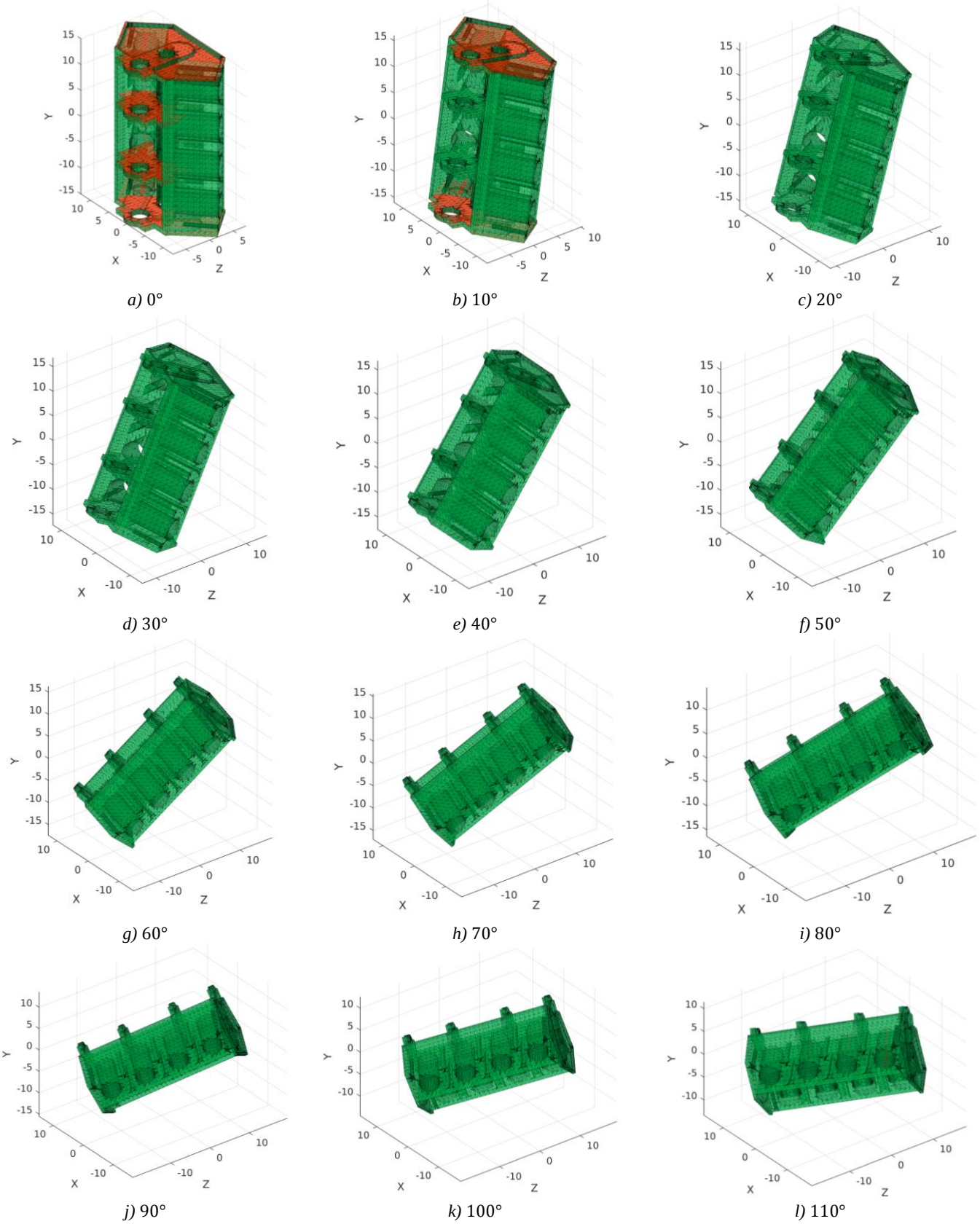

a) 0° *b)* 10° *c)* 20°

d) 30° *e)* 40° *f)* 50°

g) 60° *h)* 70° *i)* 80°

j) 90° *k)* 100° *l)* 110°

Figure 3. Orientations of test object. Surface triangles that can be properly reconstructed are shown in green, while the surfaces that cannot be properly reconstructed are shown in red.

For each orientation, a set of radiographs was generated using in-house simulation software with following parameters:

- Source-to detector distance 1060 *mm*,
- Magnification 11,
- Detector pixel size 0.2 μm,
- Detector size 2000 x 2000 pixels,
- Angular step 0.1°,
- Monochromatic point-like X-ray source.
- No noise or blur was added to simulated radiographs.

Reconstruction was performed in Nikon CT PRO software. No additional corrections were applied to the datasets. Surface determination with sub-voxel resolution, visualization, and measurements were performed in VGStudio MAX (VolumeGraphics GmbH, Germany).

3.1 Nominal-actual comparison

Different orientations of the object in the measurement volume are illustrated in figure 3. Surface triangles that can be properly reconstructed are shown in green, while the surfaces that cannot be properly reconstructed are shown in red. For views *c-l* percentage of surface affected by cone-beam artifact is quite low. CT system operator can rotate and zoom-in to check which features are affected by artifact. Coarse mesh was used for visualization only.

For each orientation, we compared output of full CT simulation (extracted surface) against the STL file. In figure 4 we show results of nominal-actual comparison for some orientations of the test object. In figure 4a, top row, results of nominal-actual comparison for the initial orientation (0°) of the object are shown. One can see that, all planes suffer significantly from cone-beam artifacts; in particular, the top and bottom planes appear to be incomplete. Cone-beam artifacts are also evident on the inside of the top and bottom shafts (shown as thin blue stripes on the right side of figure 4a), which are captured by the output of our proposed method (figure 4a, bottom row). In figure 4b we show the 12th orientation of the object, which corresponds to the 110° rotation. On the left side of figure 4b, only holes C5 - C7 are affected by cone-beam artifacts; this observation is consistent with the output of proposed method (figure 4b, right).

It is generally stated that uncertainty in surface determination with sub-voxel resolution is within 1/10 of voxel value [3]. In table 1, we compare the results of the nominal-actual comparison and the output of proposed method. The cumulative 'corrupted' surface area in the nominal-actual comparison is shown for deviations of more than 1/10 of the voxel size. Our proposed method tends to slightly underestimate the percentage of corrupted surface. Authors believe that cone-beam artifacts are correlated with other error sources such as partial volume effects and limited precision in CT simulation.

Orientation	*Output of proposed method, number of corrupted triangles*	*Output of proposed method, % of total surface area corrupted by cone-beam artifact*	*Results of nominal-actual comparison in VGStudio MAX, % of total surface area with deviations more than 1/10 of voxel*
0°	608354	23.24	25
10°	375799	15.15	19
20°	10815	0.03	2
30°	7567	0.02	2
40°	262	0.00	2
50°	128	0.00	1
60°	50	0.00	1
70°	9	0.00	1
80°	0	0.00	1
90°	20	0.00	2
100°	1222	0.01	2
110°	20138	0.26	95

Table 1. Comparison of results of nominal/ actual comparison and output of proposed method.

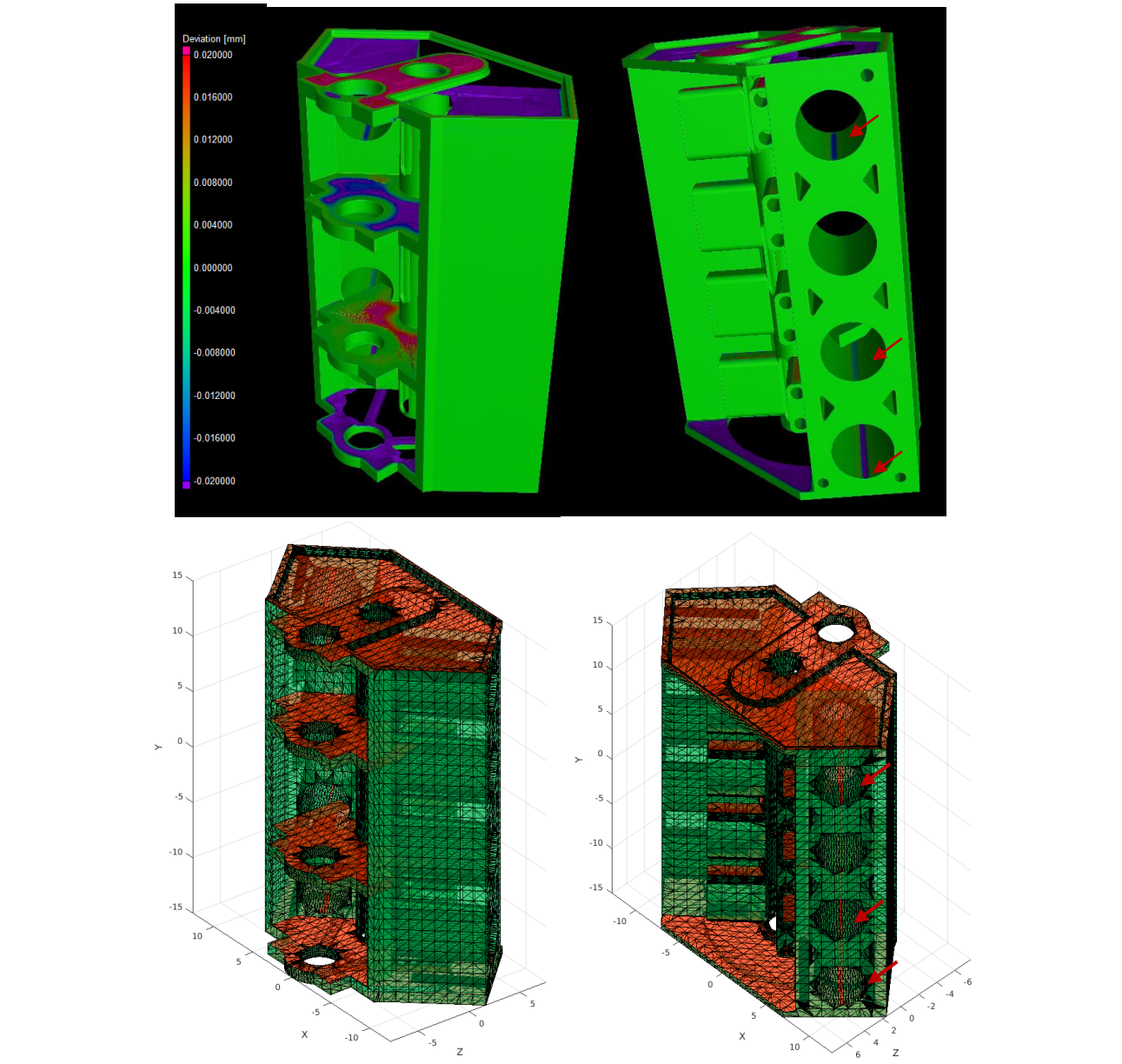

a) 0°

b) 110°

Figure 4. Results of nominal-actual comparison.

3.2 Dimensional measurements

For each orientation of the object, form errors of the following features (shown in figure 2) were measured using the minimum-zone method [4]:

- 8 holes numbered C1 – C8; holes C1-C4 have nominal radius 2.125 mm, while holes C5-C8 have 2 mm radius,
- 16 holes H1 – H16 with nominal radius 0.475 mm,
- 8 parallel planes P1 – P8.

Figure 5 shows form error for the measured features expressed as percent of voxel size. For orientations 0° – 20°, where cone-beam artifact is most pronounced, form error is very high (up to several voxels). For orientations 30° – 100°, form error stays within 20% of voxel size for the holes and 25% for the planes. In the 110° orientation, only holes C5 - C8 are affected (figure 5a), which also agrees with output of proposed method (figure 4b).

Cone-beam artifacts increase with increasing distance from the mid-plane, *i.e.* with bigger cone opening angle. Consequently, in the initial orientation of the object (0°), the top and bottom holes will be affected more than the holes located closer to the center of the object e. In figure 6, we show absolute error in hole radius for the holes C1-C8 and H1-H16. Error in radius strongly correlates to the amount of surface corrupted in the specific feature. That is, for the top and bottom holes (C1, C4, C5 and C8), where cone-beam artifacts are more pronounced, error is very high for the first two object orientations. For the holes closer to the object center (C2, C3, C6 and C7), the error in the first two object orientations does not exceed errors observed in the other orientations. Similar observations were made for holes H1-H16. However, since holes H1-H16 are not as distributed along the vertical direction as C1-C8, *i.e.* the holes H1-H16 occupy smaller cone opening angles, the magnitude of observed errors is smaller.

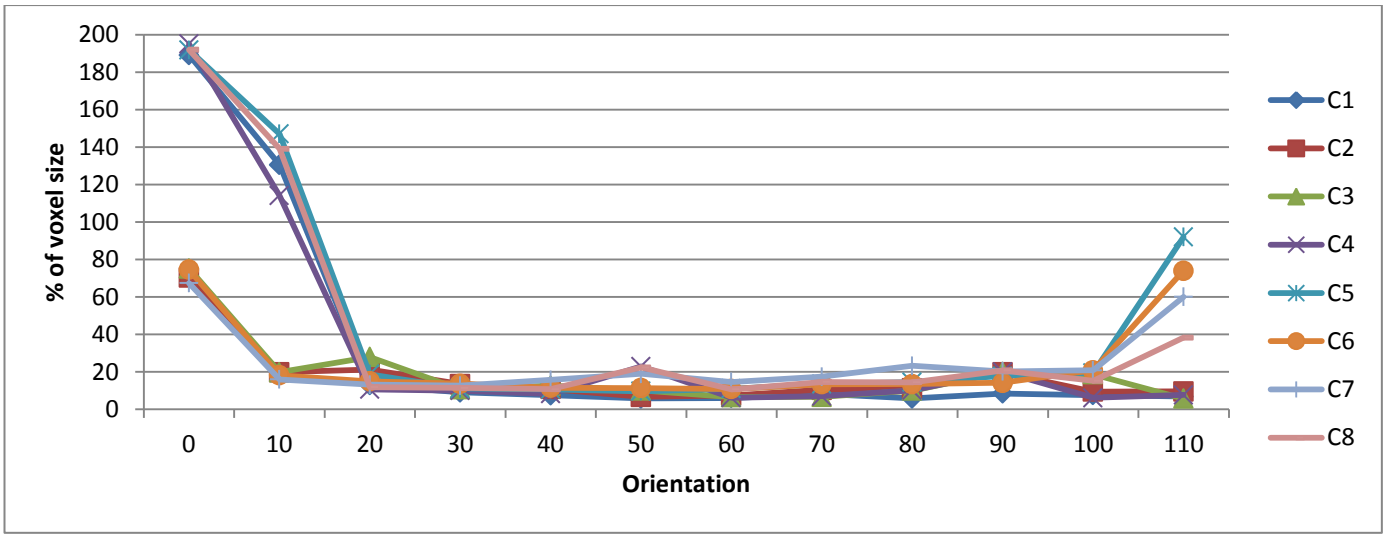

a) Form error for holes C1 - C8

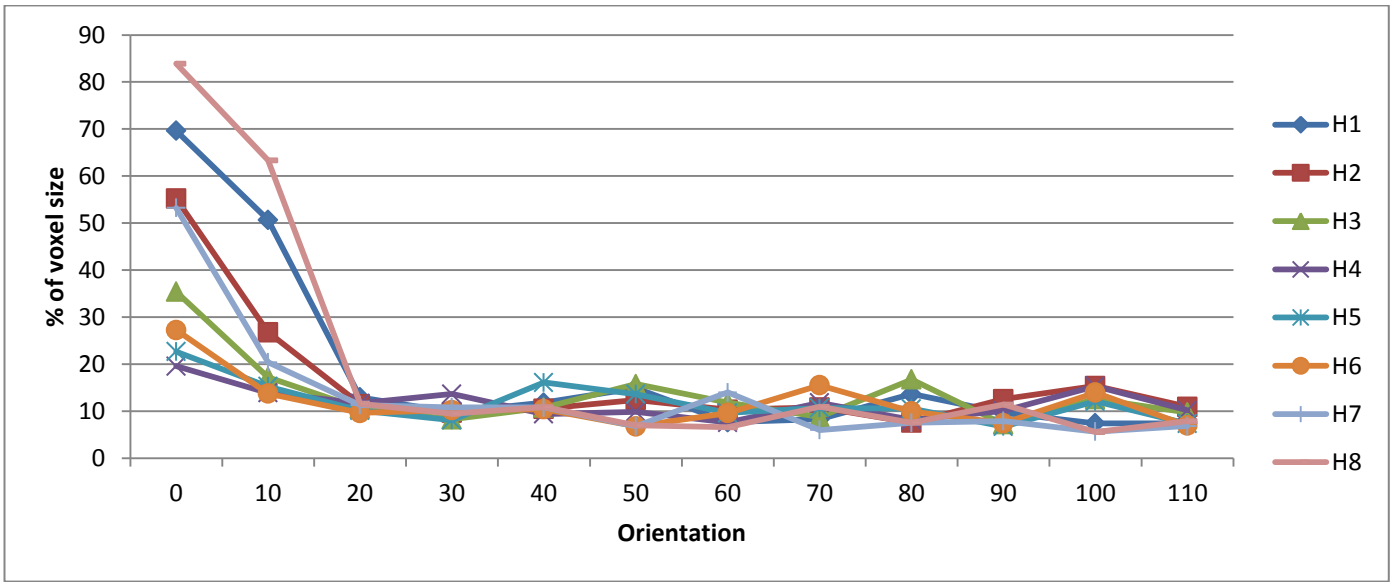

b) Form error for holes H1 - H8

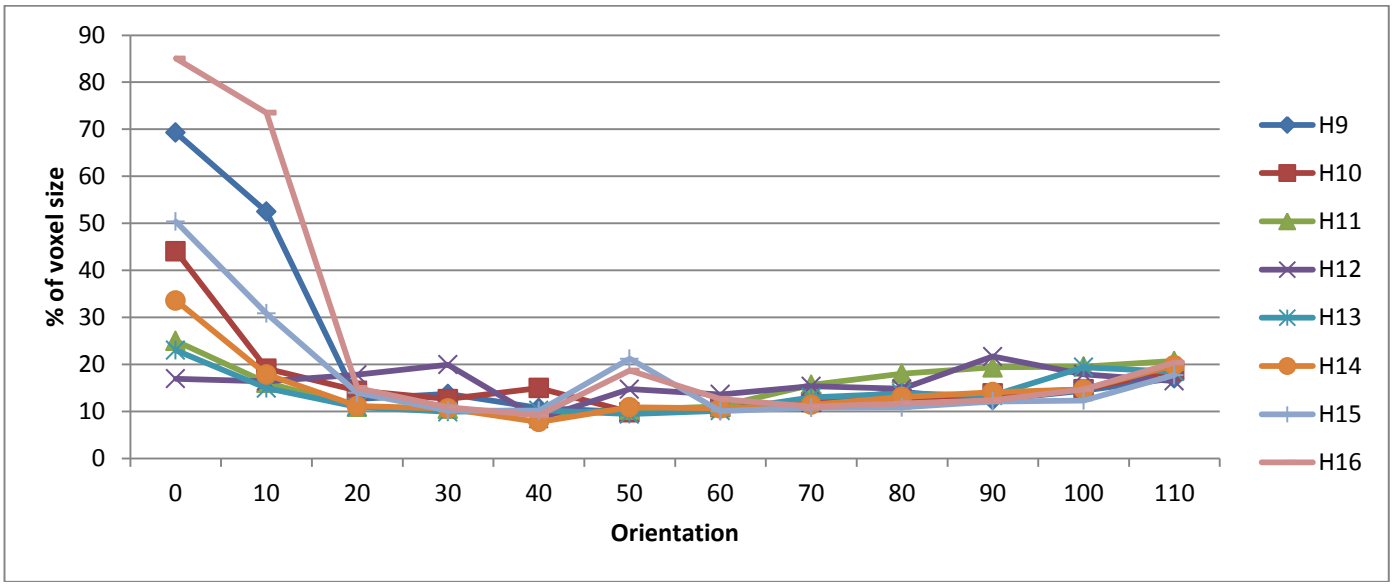

c) Form error for holes H9 - H16

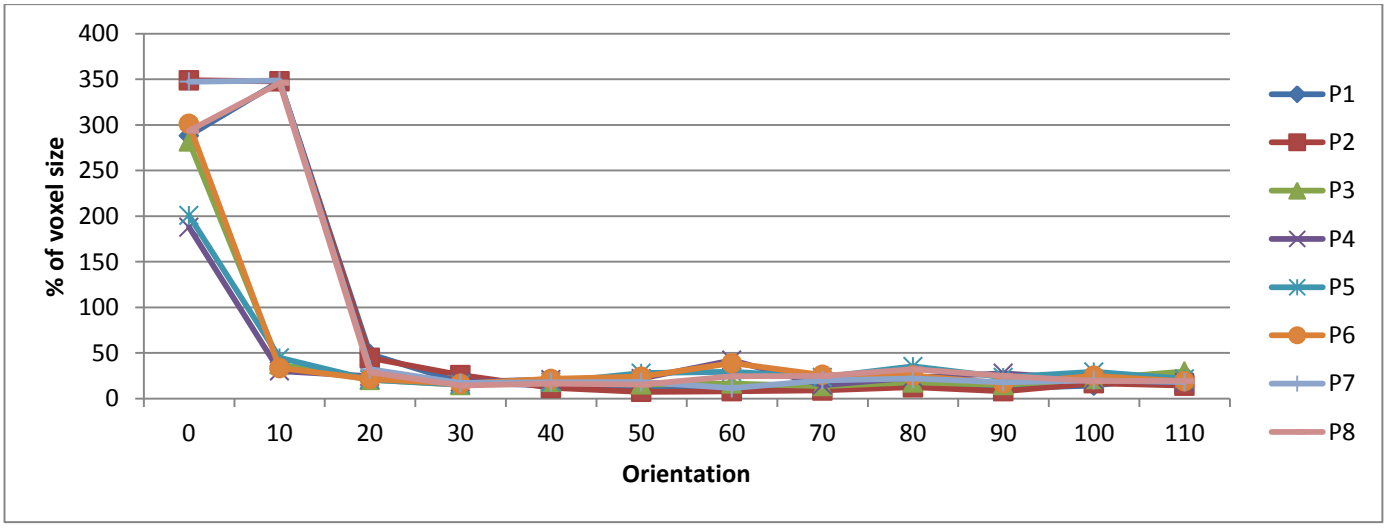

d) Form error for planes P1 - P8

Figure 5. Form error measurement results.

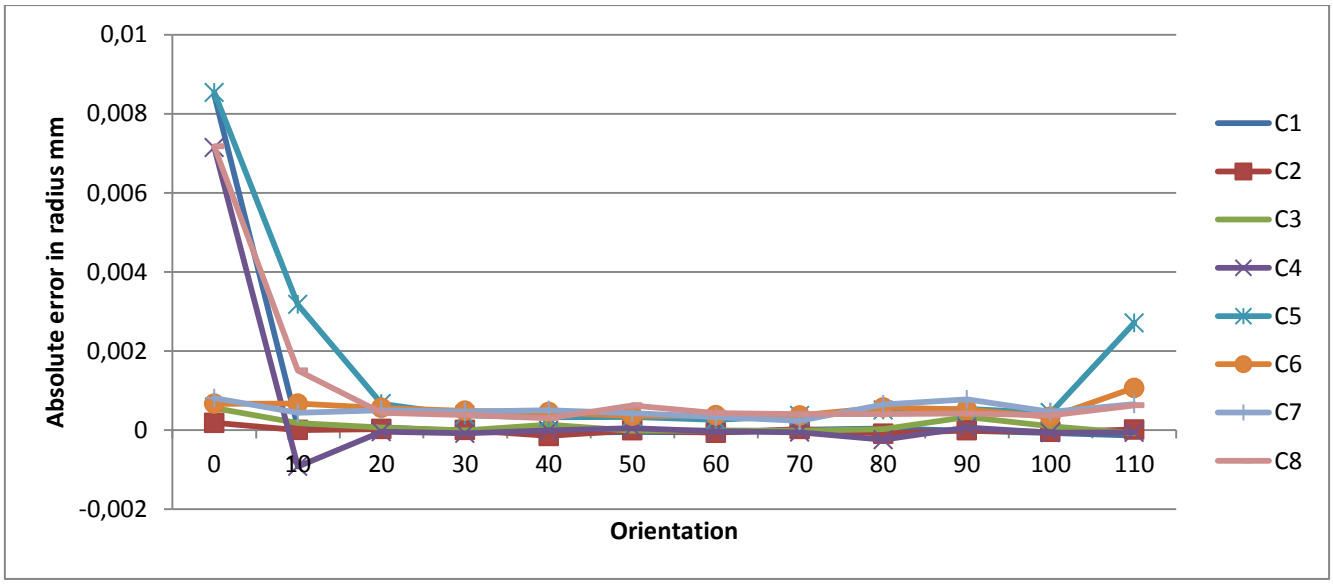

a) Absolute error in radius for holes C1-C8

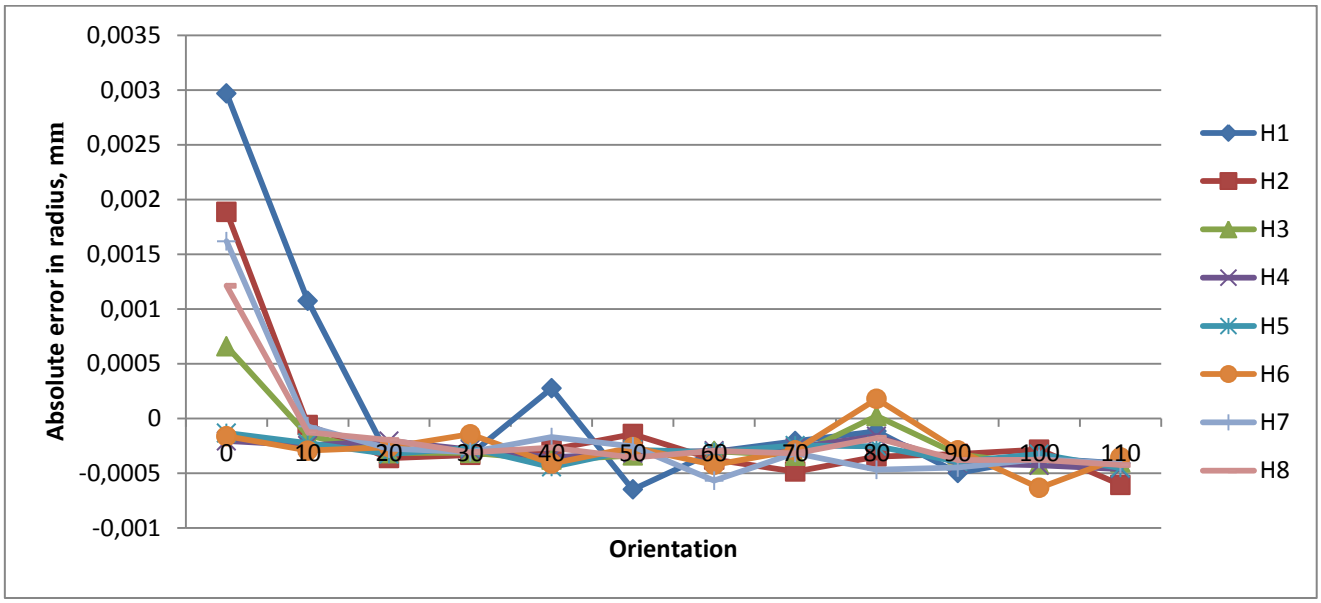

b) Absolute error in radius for holes H1-H8.

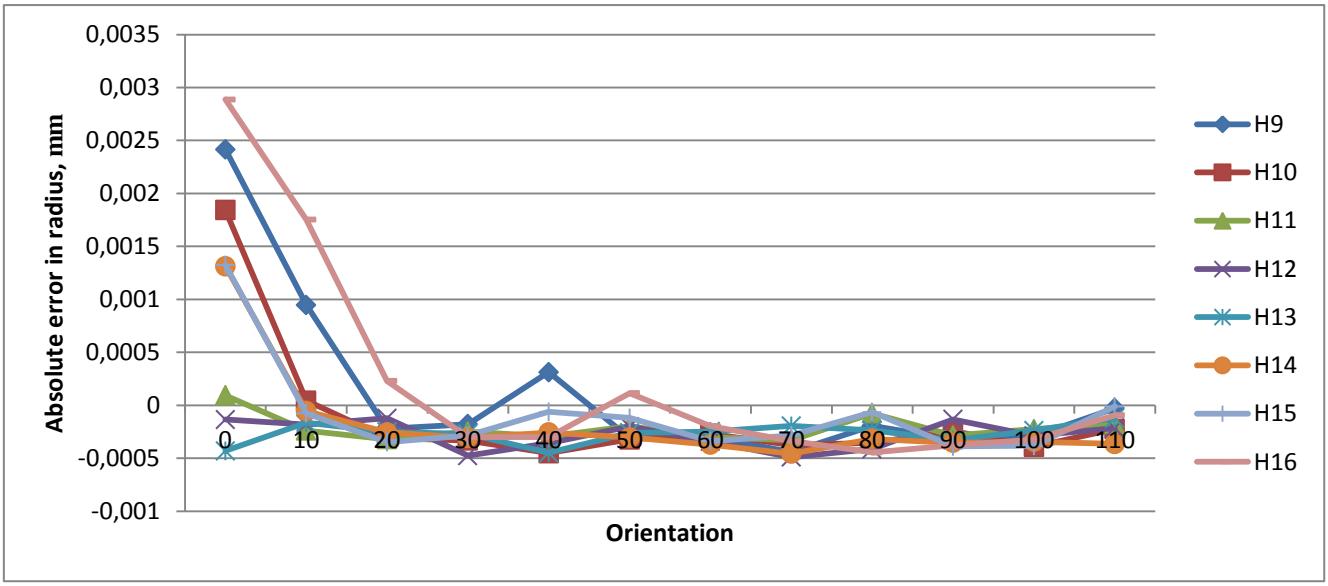

c) Absolute error in radius for holes H9-H16

Figure 6. Radius measurement results

4 Conclusions

Cone-beam artifacts can significantly affect the quality of CT reconstructed surfaces. Since appearance of these artifacts depends on the object itself, general correction procedure cannot be applied. However, the influence of the cone-beam artifacts can be significantly reduced if the object is appropriately oriented. In this paper, we present a method to evaluate the influence of cone-beam artifacts on segmentation results. The method can be used for visualization of cone-beam artifacts on surface reconstruction and for determining the optimal orientation of the object to minimize the presence of such artifacts. Since the algorithm used to implement method evaluates every triangle separately, it is well suited for parallel processing.

References

[1] H.K. Tuy, An inversion formula for cone-beam reconstruction. SIAM Journal on Applied Mathematics, 43(3), 546-552, 1983

[2] S. Bartolac, Intrinsic Artefacts of circular cone-beam computed tomography, Doctoral dissertation, University of Toronto, 2009

[3] S. Carmignato, Accuracy of industrial computed tomography measurements: experimental results from an international comparison. CIRP Annals-Manufacturing Technology, 61(1), pp.491-494, 2012.

[4] G.T. Anthony, Chebyshev reference software for the evaluation of coordinate measuring machine data, 1993